EUROfusion

EUROFUSION WPDTT1-PR(16) 16271

R Zagorski et al.

Evaluation of the power and particle exhaust performance of various divertor concepts for DEMO

Preprint of Paper to be submitted for publication in
Nuclear Fusion

This work has been carried out within the framework of the EUROfusion Consortium and has received funding from the Euratom research and training programme 2014-2018 under grant agreement No 633053. The views and opinions expressed herein do not necessarily reflect those of the European Commission.

Evaluation of the power and particle exhaust performance of various alternative divertor concepts for DEMO

R. Zagórski[1], V. Pericoli[1,2], H. Reimerdes[3], R. Ambrosino[4], H. Bufferand[5], G. Calabro[2], P. Chmielewski[1], G. Ciraolo[5], J. Harrison[6], I. Ivanova-Stanik[1], K. Lackner[7],T. Lunt[7],S. McIntosh[6], F. Militello[6], M. Poradzyński[1], G. Rubino[2] , F. Subba[8], R. Wenninger[7], B. Viola[2], H. Zohm[7]

[1]Institute of Plasma Physics and Laser Microfusion, Hery 23, 01-497 Warsaw, Poland
[2]ENEA-Frascati, Italy
[3]EPFL, SPC, Lausanne, Switzerland
[4]Universita di Napoli, Italy
[5]CEA, St. Paul-lez-Durance, France
[6]CCFE, Culham Science Centre, Abingdon, Oxon, OX14 3DB, UK
[7]Max-Planck-Institut für Plasmaphysik, D-85748 Garching, Germany
[8]Politecnico di Torino, Italy

E-mail: `roman.zagorski@ipplm.pl`

May 2016

Abstract. To mitigate the risk that the ITER conventional divertor solution, based on a single-null (SND) magnetic configuration and tungsten (W) targets, will not extrapolate to a fusion power plant, EUROfusion is assessing alternatives including advanced configurations (AC) and the use of liquid metals (LM) as target material. The paper describes the present status of modelling activity devoted to comparing the stationary plasma exhaust properties of possible AC including LM solutions with the standard SND divertor for the EU version of DEMO, leaving out the ELM problem. Feasibility studies have been performed to demonstrate the ability of various codes to predict the basic exhaust characteristics of alternative divertor configurations, including the snowflake divertor (SFD), X divertor (XD) and Super-X divertor (SXD), for DEMO. The main objective is to establish trends in the dependence of the power and particle exhaust characteristics on the geometrical divertor characteristics, with main focus on: *a) Divertor radiation losses; b) Accessibility of detachment, c)Peak heat flux at the target*

It has been found, that the different alternative configurations do not result in significantly different volume losses with or without added impurities. In case of SFD, this is because the main changes of the divertor magnetic topology with respect to the standard single null configuration occur in a region close to the primary X point. Here, rather far from the target, temperatures are too high and neutrals density too low to drive significant volume losses, either by radiation or by charge exchange.

Simulations show that the reduction of the heat load to the target in DEMO reactor by Li ions is rather limited and accompanied by strong core plasma contamination. A

limit for Li concentration of about 15% has been found and this results is not sensitive to the Li production mechanism. Operation of the liquid lithium divertor has to be accompanied by seeding of noble gasses (e.g. Ar) to reduce heat load to the target plates and simultaneously to reduce plasma dilution allowing for higher fusion power. In the case of Sn liquid metal divertor, sputtering processes determine conditions in the divertor leading to low plasma temperature and semi-detached conditions in the divertor. In spite of high radiation fraction for Sn target ($> 82\%$), seeding with additional impurities (e.g. Ne, Ar) is necessary to reduce the power to the divertor targets to acceptable levels.

PACS numbers: 52.55.Fa, 52.55.Rk, 52.30.Ex

Keywords: DEMO, impurity, divertor configuration, edge plasma

1. Introduction

The development of a reliable solution for the power and particle exhaust in a reactor is recognized as a major challenge towards the realization of a nuclear fusion power plant [1, 2]. To mitigate the risk that the ITER conventional divertor solution, based on a single-null (SND) magnetic configuration and tungsten (W) targets, will not extrapolate to a fusion power plant, the European fusion consortium (EUROfusion) is assessing alternatives including advanced configurations (AC) and the use of liquid metals (LM) as target material. The exhaust problem comprises the removal of heat and particles from the magnetically confined plasma. While neutrons deposit their power in a large volume, the power transported by charged particles, energetic neutrals and radiation is absorbed in a thin surface layer of the plasma facing components (PFCs), where it can cause erosion and melting, polluting the plasma and damaging the armour. The power transported by charged particles is of particular concern, since the interaction area of the plasma with the PFCs is constraint by the magnetic field, which leads to locally high heat fluxes. Since the scrape off layer (SOL) width in tokamak plasmas is believed to be independent of the size of the device (e.g. [3, 4]), the exhaust power increases faster with the size of the device than the area where the plasma interacts with the wall. A fusion power plant, which will exceed the size of ITER, must, therefore, also harness a greater peak heat flux than ITER. At the same time the higher particle and neutron fluence in a reactor imposes stronger constraints on the target materials and the admissible erosion.

The ITER exhaust solution is based on a single-null magnetic configuration and tungsten (W) targets. Present target technology is capable of handling stationary heat fluxes of up to 10MW/m^2. To reduce the heat flux onto the divertor targets in the ITER $Q = 10$ scenario to tolerable values 80-85% of the 150MW of heating power must be converted into radiation and, thereby, distributed over a large surface area. This will be achieved by seeding impurities that radiate in the core ($\sim 50MW$) and in the SOL (70-80MW).

The present baseline solution for DEMO foresees a similar conventional single-null magnetic configuration and solid tungsten targets. Present technological solutions for the targets that are believed to be viable despite the high neutron and plasma fluence are expected to handle stationary heat fluxes of up to 10MW/m^2. To meet this constraint the radiated fraction, $f_{rad} = P_{rad}/P_{heat}$, has to be increased above the ITER value.

The baseline strategy has many constraints and associated risks. For stationary operation it is required that:

- the peak stationary heat flux must not exceed 5-10MW/m^2 to avoid damage of the target armour;
- the plasma temperature at the target must be below 5 eV to avoid excessive W sputtering;
- the power flux across the separatrix in the plasma channel must be compatible with H-mode operation;

- the exhaust solution must be compatible with sufficient core confinement,

and the main uncertainties are shortly:

- scaling of power decay length to DEMO predicts a possible tiny power flow channel for conveying P_{sep}, the power input into the SOL;
- the consequent need for a high radiated power fraction in the bulk, questionable for a (robust) H-mode operation, confinement quality and also for an acceptable control of P_{sep}; since a small fractional variation could imply a very large one for P_{sep};
- stability of detachment under high heat fluxes;
- ability to sufficiently suppress transients/possibility to handle not fully mitigated transients;
- lifetime issues due to long term plasma impact and neutron irradiation.

There is doubt that the current baseline solution based on a single null divertor and solid tungsten targets can simultaneously meet these constraints and mitigate the risks. Therefore, alternative solutions are being seeked in parallel to the baseline solution, to increase the allowable range of parameters, such as the power crossing the separatrix in the plasma channel, P_{sep}, the upstream density, $n_{e,sep}$, and the impurity concentration, typically evaluated at the outboard midplane, $n_{z,sep}$. The promising concepts include several alternative magnetic divertor configurations (ACs) [6, 7, 8, 9, 10] and liquid metal (LM) divertor targets [11, 12, 13, 14, 15, 16, 17].

In particular, the following advanced magnetic configurations (AC) have been considered in our studies: X divertor (XD), Super-X divertor (SXD) and Snowflake divertor (SFD) (see Sec. 4.1).

The approach presented in this paper to assess solutions for DEMO divertor consists of a comparison of the selected new divertor concepts with the baseline exhaust solution which is based on direct extrapolation of ITER divertor solution to the DEMO reactor. Boundary parameters and technological capabilities for DEMO are presently still very uncertain, with ITER being an essential step to improve the accuracy of predictions and present study can, therefore, only seek to evaluate the potential of alternatives compared to the conventional solution, thereby, reducing the effect of any systematic errors in absolute predictions.

2. Experiments

It should be noted, that different power exhaust solutions have been already investigated in various existing tokamaks TCV [22, 23, 24], NSTX [27, 28, 29], FTU [11, 12, 13, 14, 15, 16], DIII-D [30, 31] and EAST [32]. It was first demonstrated at TCV tokamak [23] that snow-flake divertor configuration is compatible with the high confinement H-mode regime. It is evident from the TCV experiments that the SFD configuration leads to the increased cross-field transport mechanism which may be related to the increased

convection driven cross-field transport in the null-point region[25], $E \times B$ drifts[26] and increase of the radial gradients.

Recent DIII-D studies [31] show that the snowflake SFD enables significant manipulation of divertor heat transport for power spreading in attached and radiative divertor conditions, between and during edge localized modes (ELMs), while maintaining good H-mode confinement. Experimental results are very interesting but require careful analysis to confirm the role of other physical mechanism against flux expansion effects.

NSTX results demonstrated [28, 29] that a SFD configuration could be generated with two divertor coils, and that SFD showed a higher divertor volumetric power and momentum losses, and led to reduced peak divertor heat flux, core impurities and radiated power while good H-mode confinement was maintained.

Experiments at EAST demonstrated the possibility of creating and controlling two-null divertor configuration on a large superconducting tokamak. First two-null divertor experiments (called quasi snow-flake - QSF) have been devoted to investigate a configuration with a significant distance between the two nulls at low plasma current. These EAST experiments are an important preparatory step for the analysis of XD and SFD, but the results so far are mainly based on flux expansion.

During the experiments performed on NSTX in 2010 [17],$\sim$ 0.85 kg of Li was evaporated onto the NSTX PFCs where a 50% reduction in heat load on the Liquid Lithium Divertor (LLD) was observed, attributable to enhanced divertor bolometric radiation. This reduced divertor heat flux through radiation observed in the NSTX LLD experiment is consistent with the results from other lithium experiments and calculations. With an liquid lithium (LL) coating, the Li is evaporated from the divertor strike point surface due to the intense heat. The evaporated Li is readily ionized by the plasma due to its low ionization energies, and the ionized Li ions can radiate strongly, resulting in a significant reduction in the divertor heat flux. Due to the rapid plasma transport in divertor plasma, the radiation values can be significantly enhanced. This radiative process has the desired function of spreading the focused divertor heat load to the entire divertor chamber facilitating the divertor heat removal. The LL divertor surface can also provide a "sacrificial" surface to protect the substrate solid material from transient high heat flux such as the ones caused by the ELMs. It should be noted however, that wall conditioning and power exhaust with liquid metals are two different issues and in the present paper we focus on power exhaust only.

Since the end of 2005 most of the plasma-wall interaction experiments on FTU have been focused on the possible use of liquid lithium limiter (LLL) employing a capillary porous system (CPS) [11, 12] to investigate the physical and technological aspects related to the use of liquid metal as the plasma facing material. The main effects of lithium-coated walls are the nearly complete suppression of D_2 wall recycling and the strong reduction of light impurities such as carbon and oxygen.

In particular, during the year 2007 experiments strongly peaked density profiles were obtained [13] with lithium which are similar to those of pellet fueled discharges.

This new density regime is strictly correlated with the presence of a MARFE and a strong density gradient at the plasma edge. With lithium it has been possible to extend plasma operation at very high densities and 30% beyond the Greenwald density limit. From the technological point of view, very good indications come from the use of LLL with tungsten fibre-based CPS. The LLL is able to withstand average thermal loads up to 5MW/m^2 for about 300ms and peak values greater than 10MW/m^2. In view to extend the LLL operating regime up to 10MW/m^2 and to prevent overheating of Li surfaces the Cooled Lithium Limiter (CLL) has been installed recently on FTU [16] and the first experiments with plasma have been successfully performed. CLL has been inserted up to the last closed magnetic surface without any damage. No droplets have been observed by visible camera in 30 shots at different plasma conditions and CLL positions. From the surface temperatures monitored by a fast infrared camera and the ANSYS code simulations, heat loads up to 2 MW/m^2 have been withstood by the limiter for more than 1 sec.

Today's experiments operate with SOL conditions that are very different from those expected in DEMO and direct extrapolation of the experimental results to DEMO is not justified. Therefore dedicated experimental and modelling effort is necessary to bridge the gap between present day experiments and DEMO and find reliable solution for the power exhaust problem.

In this paper, we discribe the status of the EU modelling activity started in November 2014 and devoted to compare the properties of possible AC and LM solutions with the standard SND divertor for the EU version of DEMO [33] under steady state conditions, leaving out the ELMs problem. Feasibility studies have been performed to demonstrate the ability of various codes to predict the basic exhaust characteristics of alternative divertor configurations for DEMO.

3. Description of the baseline solution

The baseline DEMO concept that is being developed by the EU determines the relevant parameter regime and serves as the reference solution, which any alternative solutions must be compared against. The baseline concept consists of a single null diverted (SND) configuration with water cooled solid tungsten (W) divertor targets [36]. The performance is based on H-mode confinement assuming that a solution to mitigate or avoid large ELMs will exist. While the parameters of the baseline DEMO are still being refined, the main numbers are not expected to change drastically, especially in terms of power (due to the assumption that the EU DEMO should produce 500 MW of electrical power) and major radius (essentially fixed by the ignition criterion). Consequently, a design point from March 2014, obtained using the systems code PROCESS [37], is used as reference. Key machine and plasma parameters are given in table 1. These numbers are indicative of the 'conservative' EU DEMO design, assuming a relatively low β_N and a modest confinement improvement of $H = 1.1$, but still a density corresponding to 1.2 the empirical Greenwald limit due to the assumption of operating with peaked density

profiles.

Table 1. DEMO reference scenario with an intermediate aspect ratio (A=3.1)[33].

Machine parameters		
Major radius	$R_0(m)$	8.77
Aspect ratio	A	3.1
Elongation	k_{95}	1.55
Volume	$V[m^3]$	2214
Power fluxes		
Fusion power	$P_{fus}[MW]$	2023
alpha - heating	$P_\alpha[MW]$	404
Aux. heating (incl. Ohmic)	$P_{aux}[MW]$	51
Effective heating power (after brems. and synch. losses)	$P_{heat,eff}[MW]$	301
Line radiation in the core	$P_{rad,core}[MW]$	151
Power crossing the separatrix	$P_{sep}[MW]$	149
Plasma parameters		
Normalised beta (total)	β_N	2.6
Temperature on axis/average	$T_{e0,i0}/ < T_{e,i} >$ [keV]	27.0/13.5
Density on axis/average	$n_{e0}/ < n_e > [\times 10^{19} m^{-3}]$	11/8.7

4. Assessment of different exhaust solutions in DEMO

The main objective of present studies is to establish trends in the dependence of the power and particle exhaust characteristics on the geometrical divertor characteristics, with main focus on: *a) divertor radiation losses; b) accessibility of detachment, c) peak heat flux at the target.*

The assessment of alternative power and exhaust solutions focuses on concepts that have a high potential to reach sufficient technological maturity in time for an implementation in the DEMO design. Concepts that are thought to meet this requirement include several advanced magnetic divertor configurations (ACs) and liquid metal (LM) divertor targets. The assessment of the alternative solutions for DEMO consists of a comparison of the selected promising concepts with the baseline exhaust solution described above. Boundary parameters and technological capabilities for DEMO are presently still very uncertain and therefore, the focus is to evaluate the potential of alternatives compared to the conventional solution, thereby, reducing the effect of any systematic errors in absolute predictions. This work aims to address the lowest order effects of alternative plasma exhaust solutions. Since such an ordering is not rigorous, the presented study is necessarily incomplete and will be refined in the future. As one of the most important approximations this work only evaluates the stationary plasma exhaust in the divertor, which is the lowest order aspect of an exhaust solutions.

4.1. Advanced Magnetic Configurations

The following advanced magnetic configurations (AC) have been considered in our studies.

X divertor (XD)

The X divertor concept (XD) implemented first in the "closed" divertor experiments of the 80ies (e.g ASDEX) [5] has been re-launched recently as a reactor option [6]. It seeks to flare the flux surfaces near the divertor targets. The flaring is obtained by decreasing the poloidal magnetic field at the target, albeit at the cost of a lower grazing angle of the field line at the targer. Typically, two dedicated divertor coils are used for each target. The flaring may introduce a mechanism that counteracts the upward movement of the detachment front and result in a more robust detachment [7, 8]. The lower poloidal field also leads to an increase in the connection length. In addition the flaring improves the potential of including gas baffles in the divertor concept. The XD is only considered as a solution for the outer leg in our studies. If the merits of the XD are confirmed, it may also be considered for the inner leg or as part of a double null. The flaring of the flux on the inboard leg, however, poses a greater challenge for the coil configuration design.

Super-X divertor (SXD)

The Super-X divertor concept (SXD) seeks to increase the total flux expansion towards the target. This is achieved by increasing the major radius of the divertor targets, R_t [9, 18]. The maximum value is usually limited by the toroidal field coils. Increasing R_t allows for an increase of the wetted area, without decreasing the grazing angle of the field lines at the target or invoking plasma physics. The increase of R_t may be combined with an increase of flux expansion as proposed in the XD concept, leading to the name "Super-X divertor". Increasing R_t allows for an increase of the wetted area, without decreasing the grazing angle of the field lines at the target or invoking plasma physics. The increase of the total flux expansion introduces a decrease of the parallel heat flux, $q_{\|}$, towards the target, which is predicted to stabilize the location of the radiation fronts.

The SXD is currently only considered as a solution for the outer leg. If the merits of the SXD are confirmed, it may also be considered as part of a double null.

Snowflake divertor (SFD)

The snowflake divertor (SFD) concept seeks to decrease the poloidal field in the vicinity of the null point by introducing a second order null point [10, 19, 20, 21]. This splits the separatrix around the null into six legs with two enclosing the confined plasma and four divertor legs. Since the exact SFD is only a point in the operational plane any real configuration is characterised by two nearby first null-points (x-points). The resulting configuration may have different topologies referred to as snowflake plus (SFD+) and snowflake minus (SFD-) depending on whether the second x-point is located in the private or common flux region of the primary, active x-point, respectively. A potentially undesirable consequence is an increase of the flux compression towards the

target (in contrast to the XD). The lower poloidal field in the null point region leads to a longer connection length and divertor volume and is expected to generate large volumetric losses.

Each one of the presented configurations including the baseline configuration can, in principle, be constructed as an up-down symmetric configuration. In the case of two conventional divertors the resulting configuration is usually referred to as a double-null divertor (DND). The DND is not treated in this paper but may be considered in the future studies as it may be a solution for the inner targets. In addition it has recently gained more attention as it addresses the problem of heat loads onto the ceiling of a lower SND device, which usually limits the SOL and experiences greater heat loads than any other region of the main chamber.

The feasibility of advanced magnetic configurations on DEMO depends on whether there are engineering solutions to build such a device and how much it would cost. Starting from the DEMO SND baseline 2014 with aspect ratio 3.1 [33], the definition of the alternative configurations on DEMO is based on an iterative procedure composed of two main steps. In the first step, given a plasma shape that features the main characteristic of an alternative divertor concept, the geometry of the machine (first wall, vessel and toroidal field coils) is adapted to the magnetic configuration; in the second step an optimization of the PF coil system (number, position and current in the PF coils) is performed[34]. In case of the XD and SXD configurations only optimization of the outer leg has been done so far whereas for the SFDs the position of the secondary x-point is not optimized. The present set of configurations [35] under study represents only an initial step and will be revised in the future as the definition of constraints, costs and optimization criteria improves.

4.2. Modelling approach

The performance of the proposed alternative configurations is assessed using models of various degrees of sophistication. The reference scenario with power input into the SOL $P_{sep} = 150$ MW and volume averaged plasma density $\langle n_e \rangle = 8.7 \times 10^{19} m^{-3}$ is described in section 3. The present SOL modelling assumes a separatrix plasma density at the stagnation point $n_{sep} = 2.5 \times 10^{19} m^{-3}$ close to $0.3 \times \langle n_e \rangle$[38]. The codes that have been considered for this study are the couple TECXY and COREDIV [39, 40, 41], EDGE2D [42, 43] SOLPS [44, 45], SOLEDGE2D [46], EMC3-Eirene [47], OSM-Eirene [48]. However only the simpler code TECXY has so far completed the process of creating proper computing meshes for all configurations and has been used for an exploration of the possible operating parameter space around the reference scenario. The other mentioned codes at present have produced preliminary results only for SND, XD and SXD configurations and are on the way of solving the problem of the SFDs more complex meshes. Therefore most of the results presented here are from TECXY and COREDIV. TECXY is a 2D multifluid code, which takes into account the magnetic topology with some limitations: 1) of considering only two main target plates (rigorously

multiple plates should be considered for SFDs); 2) of neglecting the private flux region. Furthermore the neutrals are treated analytically rather than as a fluid or with a Monte-Carlo computing technique. The absence of the Monte-Carlo statistical approach allows to neglect the real geometry and making the computing mesh cells with two sides perpendicular and two parallel to the poloidal field everywhere. The lack of any cell deformation near the target makes the calculations in these regions significantly faster. The effect of the poloidal tilting of the targets on the magnitude of the fluxes is recovered through simple geometrical transformations. We should note, however, that details of the neutral properties are quite approximate and situations where the neutral role is important are not reliably described, as when the plasma is significantly detached from the target plate. Nevertheless the approach to detachment is well described and its onset identified.

These appealing capabilities have been exploited to explore the operating parameter space through a scan of n_{sep} with different couples of heat ($\chi_\perp$) and particle ($D_\perp$) cross-field diffusion coefficients and different values of P_{sep}. The scan of the transport coefficients at P_{sep}= 150 MW and a low density of $n_{e,sep} = 1.8 \times 10^{19} m^{-3}$ guaranteeing attached conditions yields the reference couple of $\chi_\perp$ and $D_\perp$ ($\chi_\perp = 0.18$ and $D_\perp = 0.42 m^2/s$) that corresponds to an upstream e-folding decay length of the power flowing channel on the outboard equator $\lambda_{q,u} \approx 3mm$. The decay length $\lambda_{q,u}$ is here derived from the equatorial radial decay of the quantity $n_e \times T_e^{3/2}$ (see Fig.1). Considering lower values would raise concern on the validity of the code results, since the fluid modelling requires a scale length not shorter than the poloidal gyroradius.

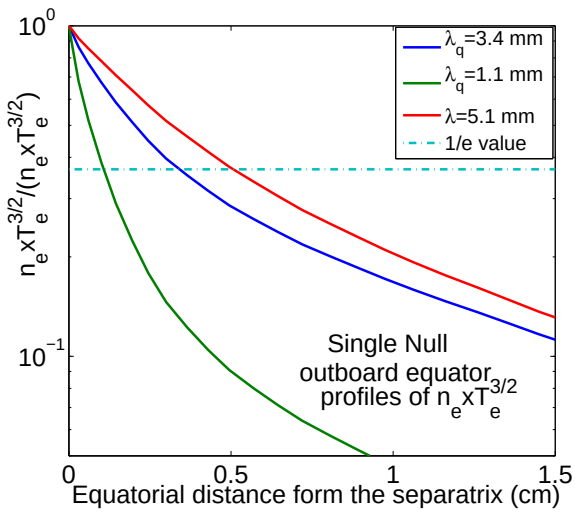

Figure 1. TECXY predictions for the equatorial profiles found for $n_e \times T_e^{3/2}$ in the SND configuration with $n_{e,sep} = 1.8 \times 10^{19} m^{-3}$, P_{sep}= 150 MW for the three fixed couples of transport coefficients, $(D_\perp, \chi_\perp)$ = (0.32, 0.12), (0.42, 0.18) and (0.5,1.0) m^2/s.

Figure 2 shows the divertor region of the computing mesh for the reference configuration and the four assessed alternatives, whereas in the figure 3 the values

of the connection length in the outer regions are plotted versus the distance from the separatrix, mapped along the outboard equator. Due to the constraints of the TECXY code the values of the connection length of the SFD are slightly over estimated. The difference in the connection length is particularly large for the SFD-, since the magnetic flux surfaces between the x-points are "bend" towards the outer target.

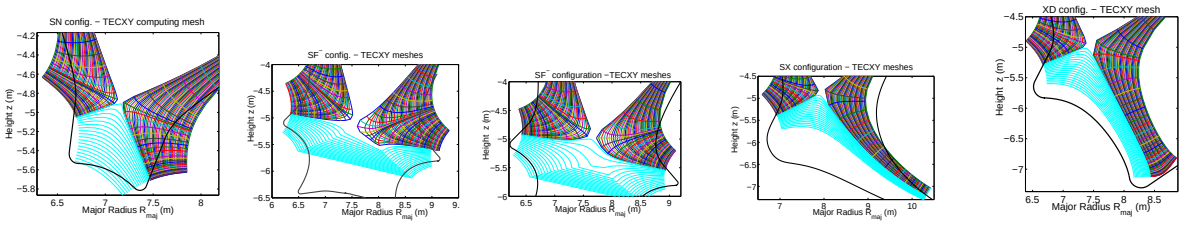

Figure 2. TECXY computing meshes for the (a) SND (standard), (b) SFD minus, (c) SFD plus, (d) SXD and (e) XD configurations. The private region mesh, not considered by TECXY, is shown in light blue.

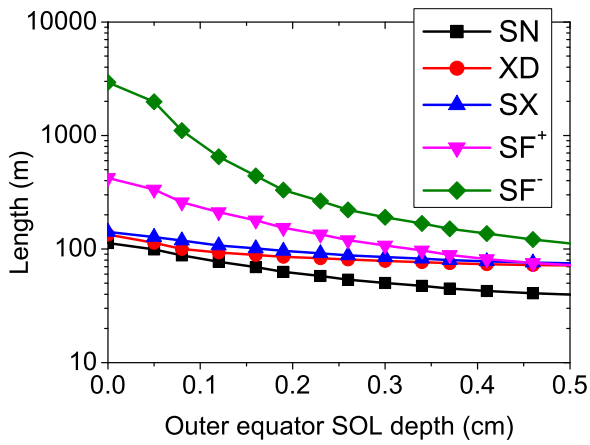

Figure 3. Outer connection length of the TECXY meshes.

4.3. Divertor performance

The work was oriented in two directions. An initial scoping study considers only pure deuterium plasmas and is devoted to identify the peculiarities of each configuration and to establish the general trends over the spanned parameter space. However, since any solution for DEMO will likely include some impurity radiation, the assessment is mainly based on calculations with various levels of impurity seeding for a fixed core scenario (i.e. fixing P_{sep} and $n_{e,sep}$). The exhaust performance of the alternative configurations is quantified by the amount of impurities needed to obtain access to a detached divertor regime, section 4.4, and to reduce the peak heat load at the target to a tolerable value (q_{max} =10 MW/m^2), section 4.5.

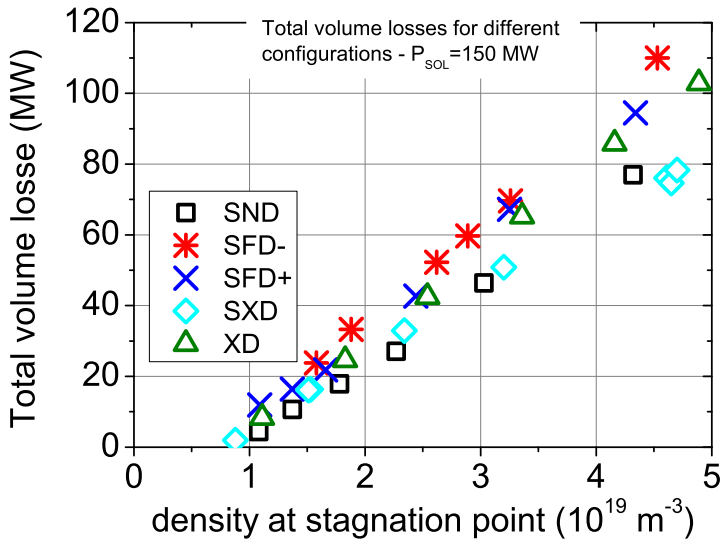

Figure 4. Total volume losses for the various configurations versus SOL density at the stagnation point.

The first question that is addressed is by how much the total power losses inside the SOL volume, P_{loss}, differs among the configurations. The outcome of the exploration activity was that in no circumstances the difference is significant. Slight difference is found only at the highest densities, perhaps not very realistic. As shown in figure 4, all configurations show no or only a small increase of P_{loss} compared to the SND, differently from previous TECXY results on smaller machines [61, 62, 32]. In the previous studies the longer connection length of alternative configurations was identified as the reason for enhanced losses. The reason why this does not occur (about 20 fold increase for SFD, see figure 3), is that almost all the difference develops in regions close to the X point where temperatures are largely unfavorable for the loss processes and neutral densities are predicted to be low. This is shown in figure 5 that plots the increment of the total connection length per unit step in the poloidal plane, i.e. $dL_{c,tot}/dL_{pol}$, versus the poloidal distance from the X point, i.e. proceeding towards the target. Only the SFDs differ substantially from the SND substantially, with SFD- showing a huge increment in the region in between the two nulls of the poloidal field, where B_{pol} is very low. The longer particle dwell time in this region leads to significantly lower plasma temperatures in the divertor region should allow a much deeper radial diffusion as shown in figure 6, where the temperature along the separatrix on both sides of the main X point in the outer divertor is plotted. The decay rate for SFD- is much faster than for the other configurations.

SFD- also leads to a wider spreading of the heat load onto the target surface is shown in figure 7. A peak load as low as 5 MW/m^2 is found for SFD-, whereas for all the configurations it is well above q_{max} (=10 MW/m^2). It should be, however, noted that in our studies the grazing angle of the magnetic field at the target is fixed and therefore also the effective poloidal flux expansion (ratio of distance along the target

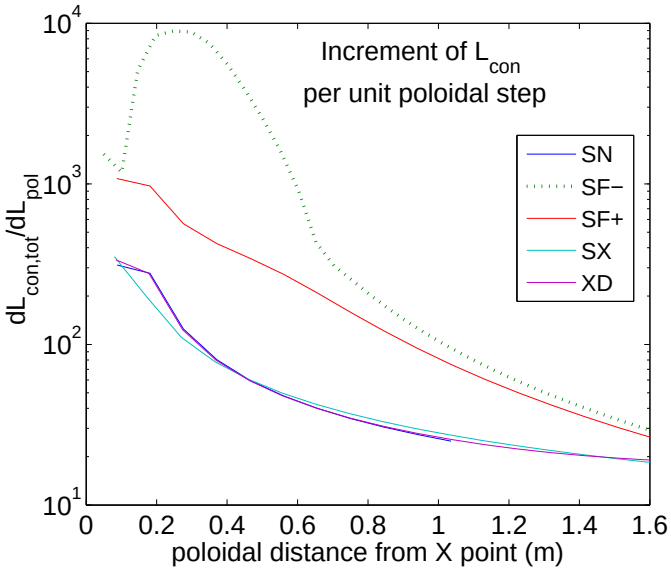

Figure 5. Increment of the total connection length per unit poloidal step in the outer divertor region vs. the poloidal distance from the X point towards the target.

and distance upstream). This decrease of the peak heat flux is the consequence of a significant broadening of the SOL in the SFD- configuration. This broadening of the SOL may result from the much lower target temperature restricting the parallel heat conduction [51] consistent with observations in JET and ASDEX-u Upgrade [50]. Further studies will have to clarify the exact reason for this behavior and also have to address the role of the neutrals in the regime of very low temperature, which has been pointed out as a limitation of TECXY above.

The corresponding loads onto the inner target are shown in figure 8. Peak heat fluxes onto the inner target are largely unchanged with SFD- and SXD showing somewhat lower values than the SND baseline. The decrease of the peak heat flux on the outer target of the SFD- is, therefore, not obtained on the expense of the inner divertor. Considering then a figure of merit for the load mitigation, we can refer only to the most critical target, which can be taken as the outer one for all configurations except for the SFD-. As far as the detachment is concerned, the present conventional limit for the electron temperature onto targets at the strike point is fixed to 5 eV. It is reached with SFD- at the lowest value of $n_{e,sep} \approx 3 \times 10^{19} m^{-3}$, whereas the other configurations require $n_{e,sep}$ up to $4.5 \times 10^{19} m^{-3}$. The first runs with SOLPS for SND, XD and SXD confirm that detachment at the nominal density of $2.4 \times 10^{19} m^{-3}$ cannot be attained without impurities.

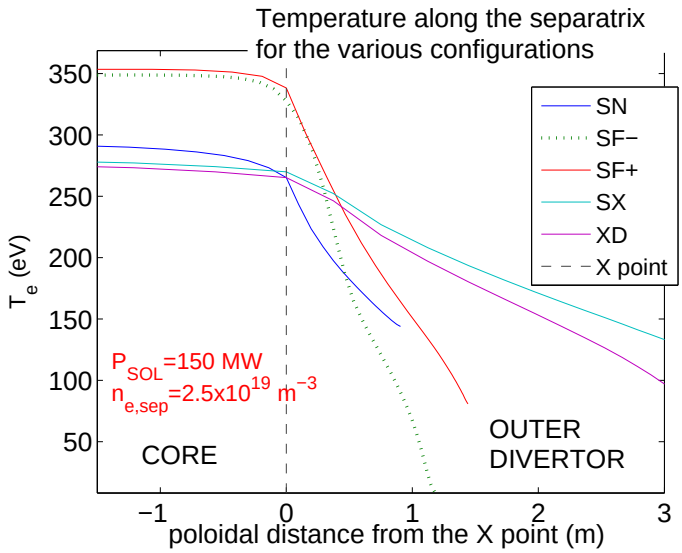

Figure 6. Variation of the electron temperature along the separatrix. The outer divertor entrance is set at $x = 0$.

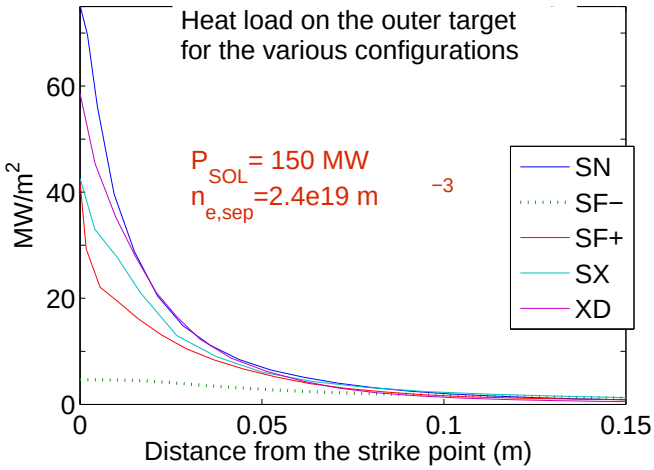

Figure 7. Power load on the outer divertor target for the various configurations. P_{sep}=150 MW, $n_{e,sep} = 2.4 \times 10^{19} m^{-3}$.

4.4. Impurity concentration needed for the onset of detachment

The effect of injecting impurities has been studied for the reference parameters: P_{sep}= 150 MW, $n_{e,sep} \approx 2.5 \times 10^{19} m^{-3}$, by simulating argon puffing in the outer divertor leg, with rates up to the maximum allowed by the numerical code stability. The effect of Ar seeding on increasing the radiation losses is shown in figure 9 and figure 10 for all configurations. In figure 9 the total target (inner+outer) load is plotted versus the effective plasma charge Z_{eff} at the stagnation point. Figure 10 shows the electron

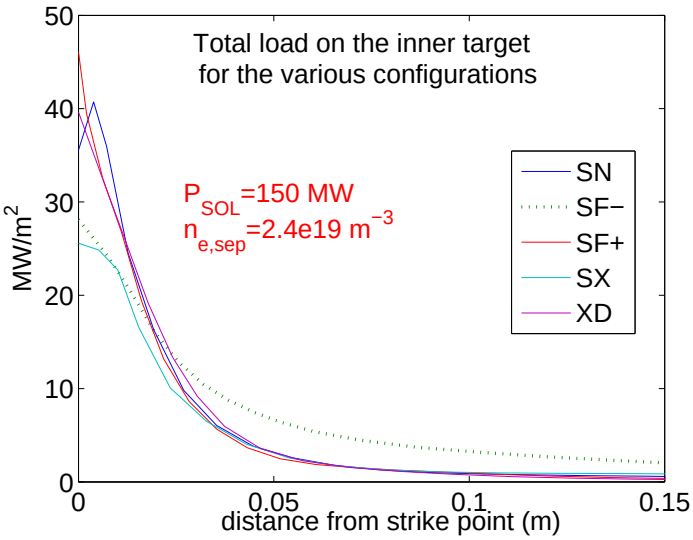

Figure 8. Power load on the inner divertor target for the various configurations. P_{sep}=150 MW, $n_{e,sep} = 2.4 \times 10^{19} m^{-3}$.

Table 2. Start of detachment - P_{sep}= 150 MW, $n_{e,sep} \approx 2.5 \times 10^{19} m^{-3}$.

					for $T_{e,strike} = 5eV$ (or $T_{e,strike} = T_{e,min}$ if $T_{e,min} > 5eV$)
Config.	$T_{e,min}[eV]$	$n_{Ar}/n_e[\%]$	$n_{Ar}[10^{17}m^{-3}]$	$\langle Z_{eff} \rangle$	Total targed load [MW]
SND(OT)	4.1	2.5	7.8	2.8	23.7
SFD-(OT)	3.2	1.9	5.7	2.5	45.1
SFD-(IT)	4.3	2.3	6.8	2.8	27.5
SFD+(OT)	5.1	2.5	7.2	2.9	33.3
SXD(OT)	8.9	2.6	7.1	2.8	24.7
XD(OT)	4.3	2.6	7.8	2.8	28.4

temperature at the outer target strike point.

As expected from pure D_2 simulations, the SFD- configuration develops slightly higher power losses, hence lower loads, but the trend is again linear for all configurations with almost the same decay rate.

In evaluating the degree of approach to full detachment we consider the most critical target, which is the outer one for all except SFD-, as anticipated above, and assume a threshold of $T_{e,strike}$=5 eV for detachment to start.

The results are summarized in Table 2. Since not all configuration attain 5 eV before code instabilities begin to develop, the achieved minimum electron temperature, is given in the 2nd column, while the other columns give the corresponding major quantities.

From this table it turns out that the SFD- is now similar to the other configurations in terms of $\langle Z_{eff} \rangle$ and total target load if we consider the most critical target. Indeed impurities are injected in the outer divertor leg while they should preferentially act on

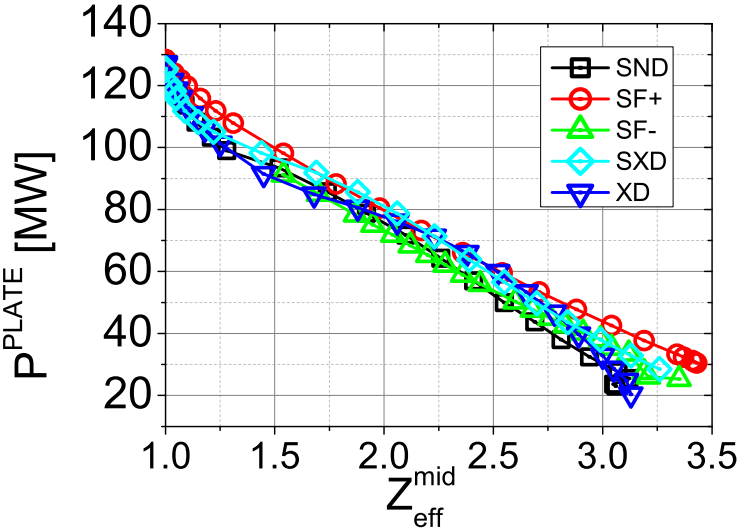

Figure 9. Total target load (inner+outer) versus Z_{eff} at the stagnation point.

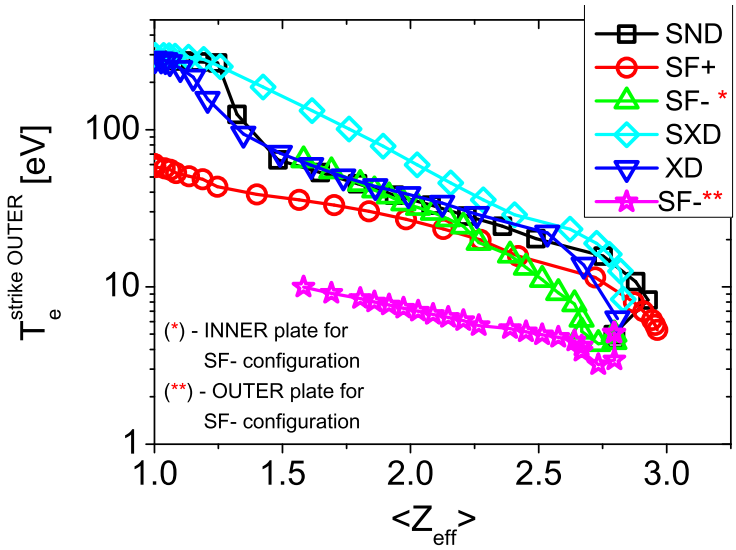

Figure 10. Electron temperature at the outer target strike point.

the quite far inner leg target. Consistently detachment starts on the outer target for SFD- at Ar concentration of 1.9 % and at $5.7 \times 10^{17} m^{-3}$ and $\langle Z_{eff} \rangle$ =2.5.

First simulations carried out with SOLPS for SND, XD and SXD, give for the Ar concentration values very much consistent with those reported in the above table. They also show that detachment is easier in XD than in the other two configurations.

4.5. Impurity concentration for required divertor power loss

If we assume that the maximum safely handled heat load is $q_{max} = 10 MW/m^2$, independently of detachment we obtain the following Table 3, where again for each configuration only the most critical target is reported, which is the outer one for all of

them except the SFD-.

Table 3. Max. allowed peak load $10MW/m^2$ - P_{sep}= 150 MW, $n_{e,sep} \approx 2.5\times10^{19}m^{-3}$.

Config.	q_{peak} $[MW/m^2]$	n_{Ar}/n_e[%] [%]	$\langle Z_{eff}\rangle$	Total targed load [MW]
SND(OT)	10.8	2.03	2.5	44
$SFD^-(OT)$	4.7	0.0	1.0	83
$SFD^-(IT)$	10.5	1.66	2.3	48
$SFD^+(OT)$	11.1	1.09	1.8	73
SXD(OT)	10.4	2.13	2.5	47
XD(OT)	11.9	1.76	2.3	50

Tolerable peak heat loads on the outer target are easiest obtained in the SFD- configuration as it requires no impurity seeding. The second best configuration is the SFD+ with Ar concentration of 1.1%, which is almost 50% lower than the concentration in the baseline solution. Note, that the SFD+ can also tolerate the highest global load (i.e. the least total volume losses), because it shows the best balances between the peak power load at the inner and outer targets

In the next figure 11 are reported the distributions of the total volume losses for the SND and SFD- configurations (upper row), and the electron temperature (bottom row) versus the poloidal distance from the main X point. The cases considered are with the maximum impurity flux that could be run. The radiating layers are always concentrated close to the target plates except for the SND case in the inner divertor leg where strong detachment occurs.

4.6. Compatibility with core performance

The results presented in the previous subsections depend on many assumptions. The robustness of either detachment or flux mitigation below q_{max} is not fully reliable with the investigation tools so far used. However the study of dependence on the input power and on the transport coefficient is underway. At present it can only be confirmed that a shorter e-folding decay length, as that predicted by the empirical scaling, $\lambda_{q,u} \approx 1mm$ [3], makes detachment, or a proper mitigation if it is the case, much more difficult. It would require a considerably larger impurity influx rate, with a consequent higher pollution of the main plasma. In turn this should induce strong core radiation and could drop the power crossing the separatrix below the threshold for the back transition from H to L mode, P_{H-L}.

This issue has been investigated with the self-consistent core-edge coupled code COREDIV for $\lambda_{q,u} \approx 3mm$, and turns out to be already quite problematic, as briefly illustrated below. The opposite is true for a faster radial transport. In figure 12 two different transport coefficients are considered: open symbols refer to the couple $D_\perp = \chi_\perp = 0.25m^2/s$, quite close to that assumed above by TECXY: $(D_\perp, \chi_\perp) =$

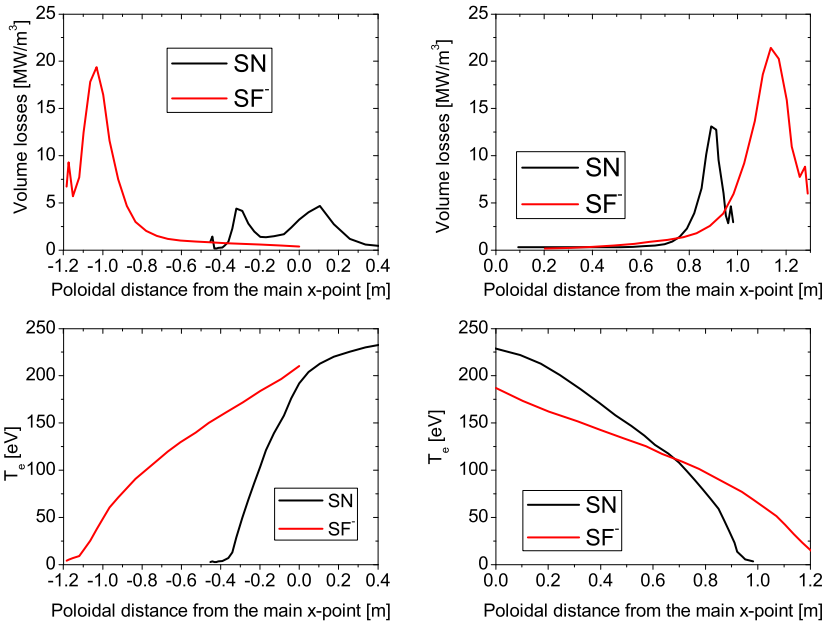

Figure 11. Total lost power density distribution (radially averaged) (upper row) and electron temperature along separatrix (bottom row) in the inner divertor leg (left) and in the outer divertor leg (right) for the SND and SFD minus configuration .

$(0.42, 0.18)m^2/s$, full symbols to a substantially faster transport, $D_\perp = \chi_\perp = 0.5m^2/s$. The figure presents versus the Ar injection rate Γ_{Ar}: a) plot of the fusion power gain Q and of the Z_{eff} core averaged value; b) plot of the power at the plate, P_{PLATE} and the power crossing the separatrix P_{sep}. Fixing attention on the open symbols (slower cross-transport) and on the abscissa where $P_{sep} = P_{H-L}$, we see that for maintaining P_{sep} above this threshold both Z_{eff} and Γ_{Ar} need to be lower and P_{PLATE} higher than the corresponding values given by TECXY for tolerable loads. Only the SFD+ approaches this limit.

The situation is much better for faster cross-field transport, where the H-L transition practically never appears. It is then consistently expected that an even slower cross-field transport, as that associated with $\lambda_{q,u} \approx 1mm$, could make the whole situation quite problematic. These calculations are of course approximate due to the nature itself of the models but indicate as critical is the full consistency between injecting impurities and unavoidably polluting the main plasma.

The above figures however also suggest that a very big fraction of the input power can be either radiated or lost by charge exchange processes without losing stability in the SOL plasma. The maximum total "volume" losses can range between 120 and 130

MW, depending on the particular configuration, corresponding to 80-85% of the SOL input power.

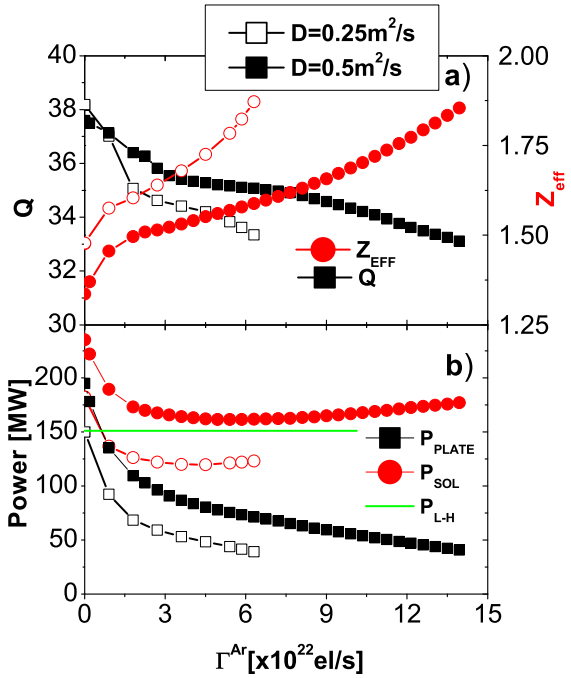

Figure 12. Versus the Ar injection rate are plotted in a) fusion gain Q (black) and Z_{eff} (red); in b) power hitting the plates (black) and crossing separatrix (red). Full/empty symbols: $D_\perp = \chi_\perp = 0.5/0.25\ m^2/s$.

5. Results from other codes

As anticipated the largest effort on other codes was focussed to create a proper computing grids to start investigations. The state of the art of each of them in relation to DEMO power exhaust calculations is briefly reviewed below.

5.1. EDGE2D modelling

As anticipated, EDGE2D - Eirene code can presently not generates meshes for alternative configurations and is, therefore, only used to verify the TECXY calculations for the SND configuration. The activity was mainly directed to point out possible differences with (or weakness of) TECXY. However, also in this case the real target geometry constrained the EDGE2D computing mesh to undergo significant deformation close to the plates. This introduced unacceptable numerical noise in the results, resembling that met by the code "OSM - Eirene" for SXD, described below. As done for this latter code, the grid was modified to become perpendicular to B_{pol} exactly as does TECXY. The advantage of this is to single out the consequences of the TECXY simple neutrals treatment distinguishing them from that induced by the the simplifications of

the target geometry. A comparison was made by assuming P_{sep}=150 MW and scanning $n_{e,sep}$ to sufficiently high values for neutrals to become non negligible, for several pairs of transport coefficients:$(D_\perp, \chi_\perp[m^2/s])$: (0.42, 0.21); (0.32, 0.12); (0.24, 0.1); (0.22, 0.08). The results are summarized by figure 13 where the peak power loads on the outer target are plotted versus the upstream separatrix density (EDGE2D in red, TECXY in blue)[52]. The agreement is very good for the transport coefficients (0.42, 0.21) being quite close to that assumed above as the TECXY reference, (0.42, 0.18). Only near to the detachment conditions (high $n_{e,sep}$) TECXY gives slightly lower values. In the case of the slower radial transport (0.32, 0.12), the TECXY predictions show higher peak heat values than EDGE2D, which can be attributed to neglecting the private flux region in TECXY.

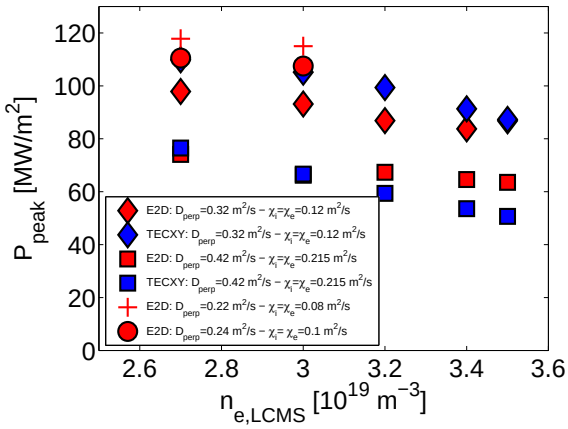

Figure 13. Peak load power onto the outer target versus the upstream separatrix density

5.2. SOLPS modelling

Since SOPLPS has currently not the capability to treat configurations with the topology of a SFD configuration, the efforts have been so far focussed on SND, XD and SXD configurations. Neutrals have been treated with a fluid model and drifts neglected as a compromise between accuracy and the speed required to build-up a modeling database. A limited scan in the upstream density and in the Ar puffing rate has been carried out. The results can be summarized as follows[53]:

(i) Without Ar seeding the limit $T_{e,strike}$ =5 eV at the outer target is never reached, also at the highest density $n_{e,sep} = 4 \times 10^{19} m^{-3}$, in agreement with TECXY.

(ii) For the no-impurity case, $T_{e,strike}$ is always quite large (> 60 eV), reduction can be large for XD, and less pronounced for SND and SXD, which again behave quite similarly.

(iii) For the code to converge, the Ar concentration upstream at separatrix must be always $n_{Ar,sep} < 10^{18} m^{-3}$ and tends towards $10^{17} m^{-3}$ at the maximum considered

value of $n_{e,sep}$. The admitted range of Ar concentration at the separatrix is consistent with TECXY estimates.

(iv) Fixing $n_{Ar,sep} = 10^{17} m^{-3}$, $T_{e,strike}$=5 eV at the outer target is much more easily with XD, at $n_{e,sep} \leq 4 \times 10^{19} m^{-3}$, than with either SND or SXD, which both require $n_{e,sep} = 4 \times 10^{19} m^{-3}$.

(v) Consistently the peak power loads are strongly reduced for XD ($> 100\times$) with Ar seeding as compared with no-seeded SND case and considerably less for both Ar seeded SND and SXD ($\approx 30\times$).

(vi) A low-temperature high radiating region is created in front of the target that extends almost to the X point for SND is somewhat reduced for XD and is quite thin for SXD. It must be evaluated how much this can affect the core plasma stability and performance.

As far as the heat load mitigation is concerned XD shows better performance than SXD, which does not show significant improvements over SND, in spite of the larger wetted area at the target.

5.3. OSM - Eirene modelling

The modelling work has been concentrated on modifying the OSM-EIRENE code for more predictive simulations. This work has been completed and has started producing results.

The main modifications to the code are:

- Each flux surface in the SOL and private flux region has $n_{e,upstream}$ and P_{heat} specified.
- Then 1D code solves the particle, momentum and ion and electron energy transport equations to calculate temperature and density profiles along each flux surface.
- Neutrals are calculated with EIRENE

Due to problems with the mesh generation code at present only preliminary results are available for SND, XD and SXD configuration and pure D_2 plasmas, but still need to be fully validated. The upstream density near the separatrix was assumed to be as close to $3.5 \times 10^{19} m^{-3}$ as possible, but numerical instabilities still limit the density at the separatrix to $\approx 3.0 \times 10^{19} m^{-3}$ for XD and to $2.87 \times 10^{19} m^{-3}$ for SXD. For this latter however the outer target profile required to be modified to avoid problems with the triangular mesh required by EIRENE. The curved surface was replaced by a flat profile, almost perpendicular to B_{pol}. Consistently with what described in the previous sections no big differences are found on the global quantities between the configurations. The loads on targets are slightly different but it is believed at present to be consequence only of the different magnetic layout. The peaks are unsustainable for all configurations with rather high T_e there ($\approx 100eV$). No sign of detachment is found.

5.4. EMC3-Eirene modelling

The effort of this modelling activity was preferentially directed to generate a proper computing mesh for the more complicated magnetic topologies, namely the SFDs. Main focus was put to the SFD-, where the closeness of the two B_{pol} nulls generates a wide region with very low $|B_{pol}|$ that makes the task quite challenging. After having completed this task, convergence problems were initially met and were overcome for some test cases with P_{sep}=150 MW through a combination of simplifying assumptions: 1) shortened divertor legs; 2) grid radial extension larger in the SOL and smaller in the confinement region; 3) reduced fueling particle rate into the SOL ($10^{22}s^{-1}$); 4) properly increased transport coefficients, well above the reference values in order to avoid problems at the strike point 2 (SP2); 5) pure deuterium plasma. However the radial extension of the grid is still to small, since a large fraction of P_{sep} escapes the outer radial boundary (up to $> 90\%$ for the highest $n_{e,sep}$ and largest values of $(D_\perp, \chi_\perp)$. Even though at this stage it is quite premature to speak of any definite characteristics, some hint of detachment is found at the strike point of the main outer separatrix. Consistently in the associate leg a strong density drop is observed. We note that this occurs just where L_{con} is greatly increased, in qualitative agreement with the TECXY simulations. Another peculiarity still to be fully investigated is that the density shows a sort of minimum at the 2nd X point, opposite to TCV behavior.

5.5. SolEdge2D-EIRENE modelling

Similarly to what has been done for ECM3-Eirene, section 5.4, also in the case of SolEdge2D-Eirene modelling, the effort of the activity was directed to generate a proper computing mesh for the more complicated magnetic topologies, namely the SFDs. Simulating snowflake divertor with transport codes remains prohibitive mostly due to the complex domain decomposition required by snowflake configurations. Indeed, most transport codes require a structured flux surface aligned grid where each x-point singularity is treated by a domain-decomposition in typically 6 zones. Adding x-points quickly increases the number of subdomains required to treat the magnetic topology. To cope with the objective of simulating snowflake divertor for DEMO, a new tool to generate grids for SOLEDGE2D-EIRENE has been developed, which is able to treat most of divertor configurations quite automatically (see Fig.14).

Mesh grids for SND, SFD plus and minus have been successfully generated and simulations with SolEdge coupled with EIRENE for simulating the neutrals have been performed for pure deuterium plasmas. The reference parameters are the following: $P_{sep} = 150$ MW, $n_{sep} = 2 \times 10^{19}\ m^{-3}$. The transport coefficients have been settled to $D_\perp = 0.3m^2s^{-1}$, $\chi_\perp = 1m^2s^{-1}$. The SFD plus configuration has been especially investigated. For the above mentioned input parameters, one finds that the secondary strike points are not very efficient in redistributing the power loads and consequently the heat load is essentially deposited on the two main strike points. More interesting

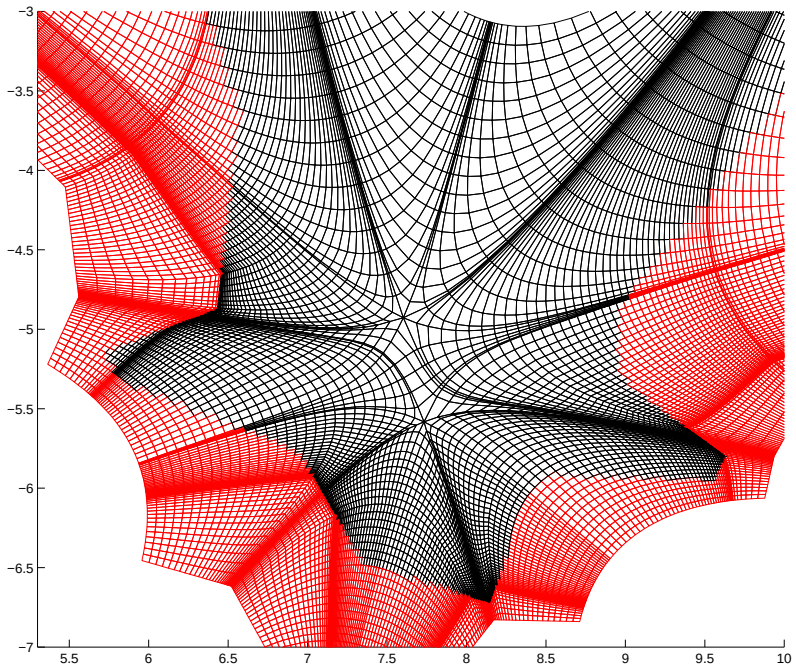

Figure 14. SolEdge2D mesh grid for a SFD plus case (enlargement of the divertor region, in black the plasma domain while in red the grid-points contained in the wall domain).

and thanks to the fact that SolEdge2D models the plasma up to the wall, both in the divertor region as well as in the main chamber, detailed profiles of plasma quantities all along the wall can be obtained which might be relevant for a detailed description of the plasma wall interaction all along the wall and not only in the divertor region, especially when the wall constraints are stringent as it is the case for large size devices as DEMO. Simulations are also running for the SND and SFD minus cases in order to have a detailed comparison between these 3 different configurations and to consolidate the results obtained with the other simulation tools presented in the paper.

6. Liquid metal plasma facing components

Power load on the divertor is one of the main problems to be solved for steady state operation on the future reactors. Liquid metals could be a viable solution for the target materials. Up to now, only liquid lithium has been extensively tested on tokamaks with very promising results, even though also other liquid metals, such as Sn, could guarantee similar or even better capability of withstanding heat loads, maybe up to tens of MW/m^2. An extended database (140 publications) on these results is contained in the final report of the EFDA power exhaust (PEX) tasks [54] aimed to assess the potential of alternative target concepts for DEMO. According to the indications coming from this report, the Capillary Porous System (CPS) has proven to be the best configuration to

confine liquid metal against MHD effects[55]. Nevertheless, if the surface temperature exceeds 500 ^{o}C, lithium evaporation becomes too strong, arising concerns about its use in a reactor [56, 57]. Of course, these attractive properties need to be verified experimentally in tokamks and problems and limitations must be recognized. Extensive experimental and modelling work is being carried on for this purpose in the USA [17, 58, 59, 60], China [63] and EU [11, 12, 13, 14, 15, 16, 49]. A major concern for the use of the liquid walls in fusion reactors is contamination of the core plasma by impurities.

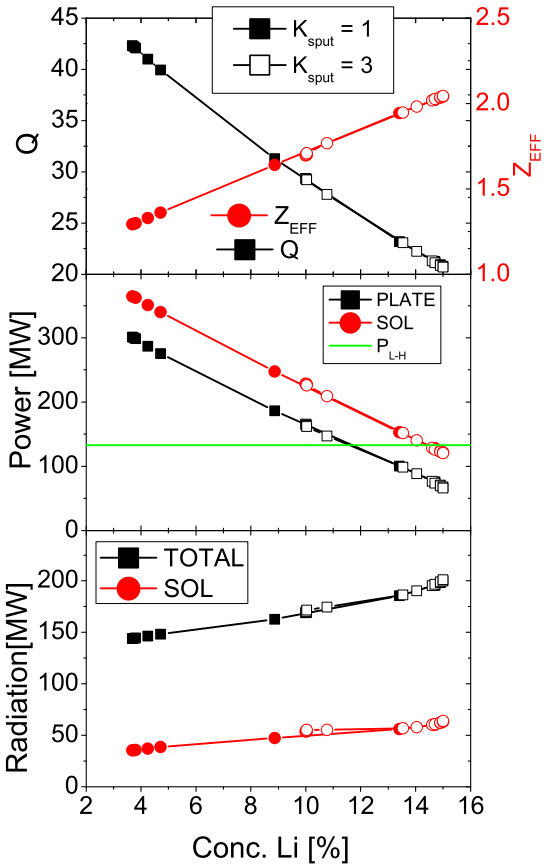

Figure 15. COREDIV simulations of Li divertor with different sputtering yields: a) fusion factor Q, b) power to the the plate and total heating power, c) total radiation and Sol radiation versus Li influx

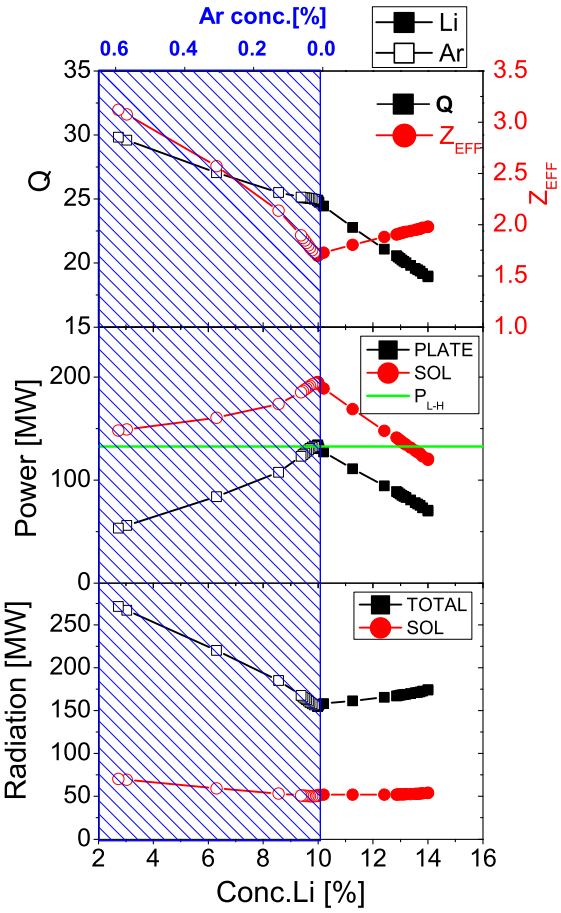

Figure 16. COREDIV simulations of Li divertor with argon seeding: a) fusion factor Q, b) power to the the plate and total heating power, c) total radiation and Sol radiation versus Li influx

6.1. Compatibility with core performance

The influx of impurities released from the liquid metal divertor might affect the core plasma performance in numerous ways and the effect depends strongly on the impurity type. The acceptable core impurity level is determined by dilution and radiation losses. For impurities with low and moderate nuclear charge Z, dilution is the dominant constraint, which would lead to the decrease of the fusion rate. If one assumes equal core densities of deuterium and tritium, $n_D = n_i/2$ and $n_T = n_i/2$, then the fusion power, P_f, is reduced by impurities via the relation [60]:

$$P_f \propto n_D n_T = \frac{n_i^2}{4} = \frac{n_e^2}{4(1 + Zn_z/n_i)} \approx \frac{n_e^2}{4}(1 - 2Zn_z/n_i)$$

where n_e, n_i and n_z are the electron, background ions and impurity ions densities, respectively. A second major factor affecting the impurity influx is whether the divertor plate has a high or low hydrogen recycling coefficient since this impacts the impurity removal efficiency.

The first simulations, both with the TECXY and COREDIV codes show that contribution of lithium to the reduction of the heat load to the target in DEMO reactor is rather limited and accompanied by strong core plasma contamination. A limit on the Li concentration of about 15% (corresponding to Li influx $\Gamma_{Li} \sim 10^{24}\ s^{-1}$) has been found above which no fusion plasma exist (Fig.15). The results are not sensitive to the lithium production mechanism, as can be seen from the Fig.15, where two different sputtering enhancement coefficient are considered. The energy losses in the case of lithium are mostly related to the synchrotron and bremsstrahlung radiation, and the divertor lithium radiation is low (< 50 MW). It should be noted that the Li concentration limit is due to reduction of the fusion power by Li contamination and by increased bremstrahlung radiation (increased Z_{eff}). For the considered DEMO parameters, the effect of strong non-coronal equilibrium radiation of lithium, as seen for example in the FTU experiments [15, 49] is unfortunately not observed.

It has been found that the operation of the liquid lithium divertor has to be accompanied by strong seeding of nobel gasses (Ar for example) in order to reduce the heat load to the target to the acceptable levels and simultaneously to reduce the core plasma contamination allowing for higher fusion energy production (Fig.16). Simulations show also, that the effect of the lithium on the plasma performance hardly depends on the particular divertor magnetic configuration. High lithium concentrations in the core plasma affect also helium transport and lead to the helium accumulation, which adds to the dilution effect. Moreover, strong dilution of the plasma in the divertor region prevents the achievement of detachment conditions in divertor.

In the case of high Z liquid metal divertor (Sn, Z=50), the effect of impurity on the plasma performance is different (Fig.17). First of all, there is very strong coupling between core and edge regions which in principle determines the operational regime of reactor. The point is that the Sn production in the divertor (due to sputtering only in presented results) strongly affects the energy balance in the core and due to

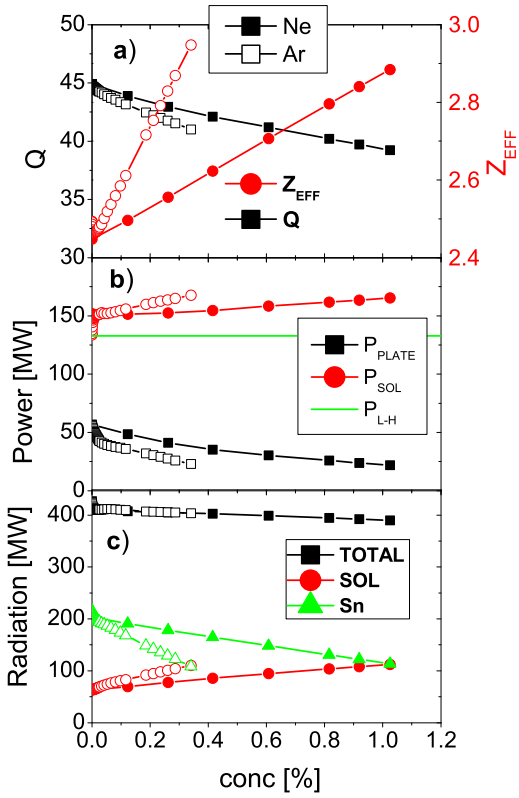

Figure 17. COREDIV simulationsof Sn divertor with neon and argon seeding: a) fusion factor Q, b) power to the the plate and total heating power, c) total radiation, SOL and Sn radiation versus seeding impurity concentration.

self-regulating mechanism, determines in turn the release of Sn atoms from LM divertor targets. Since the threshold temperature for the Sn sputtering is relatively low (5-6 eV), the conditions in divertor are such that plasma temperature stays close to the threshold temperature leading to semi-detached conditions in the divertor. It is achieved due to strong radiation of the Sn ions, mostly in the core region and the power crossing the separatrix is marginally above the P_{LH} threshold. The overall energy losses are high ($>$ 82%), but not large enough to reduce the power to the target to acceptable levels (below 40 eV). The situation improves if the seeding by low Z (Ne) or medium Z impurities (Ar) is considered. Additional radiation in the SOL regions allows for reduction of the plate temperatures below 2 eV and simultaneously strong reduction of the heat load ($<$ 23 MW) is observed. Associated with the seeding, increase of the plasma contamination (dilution) does not affect strongly the fusion performance (P_{alpha} >390 MW). In addition, the power crossing the separatrix increases ($P_{sep} > 165$ MW). The total Sn influx (Γ_{Sn}) found in the simulations vary from $\Gamma_{Sn} \sim 8.5 \times 10^{19}$ s^{-1} for the pure Sn case to $\Gamma_{Sn} \sim 6 \times 10^{19}$ s^{-1} for the cases with maximum Ne or Ar seeding. The only worry in the case of SND target is the possibility of the degradation of the energy confinement, since the radiation is localized in the pedestal region. In addition the,

accumulation of the Sn ions in the core has to be avoided by control of the impurity transport (e.g. ECRH heating[64]).

7. Conclusion

At the present stage of the study only the lowest order features of the divertor behaviour could be identified, using simple models that allow scanning a wide parameter space, still having enough accuracy for being sensitive to the actual magnetic topology. The configurations do not result in significantly different volume losses with or without added impurities. This is because the main changes of the divertor magnetic topology with respect to the standard single null configuration occur in a region close to the primary X point. Here, rather far from the target, temperatures are too high to drive significant volume losses, neither by Ar radiation, whose radiative cooling rate peaks between 20 and 30eV, nor by charge exchange.

First simulations with SOLPS show indeed that a low-temperature high radiating region is created in front of the target that extends almost to the X point for SND but is consistently reduced for XD and is quite thin for SXD. Nevertheless, prolonging by a very large amount the connection length of the power flowing channel over a sufficiently extended poloidal region can strongly favour the cross-field diffusion and therefore spread the power deposition on a sufficiently large area. This appears to happen quite well for a SFD- configuration where the secondary X point lies almost on the main separatrix and on the side of the main SOL, but it is effective also for the SFD+.

The simulations of the plasma exhaust in DEMO can be improved by

(i) including the divertor private region, which enhances the power spreading
(ii) treating more rigorously the neutrals and consistently including the real plate/divertor geometry
(iii) considering transport coefficients not constant, as usually done, but variable along a flux tube, taking also into account the possible effects of the strength of $|B_{pol}|$ and of its shear $(dB_{pol}/d\Psi)$ and of the turbulence
(iv) taking into account drifts and electric field
(v) considering self consistently the tungsten sputtering from the plates
(vi) optimizing the impurity mix
(vii) considering different locations for the impurity puffing

The present simulations of advenced configurations are, therefore, only a first step towards predictions of the plasma exhaust performance in a DEMO and applied simplifications may miss first order effects of the geometry.

Simulations with the TECXY and COREDIV codes show that the reduction of the heat load to the target in DEMO reactor by Li ions is rather limited and accompanied by strong core plasma contamination. A limit for Li concentration of about 15% has been found and this result is not sensitive to the Li production mechanism. Operation

of the LLD has to be accompanied by seeding of noble gasses (eg. Ar) to reduce heat load to the target plates and simultaneously to reduce plasma dilution allowing for higher fusion power. In the case of high Z liquid metal divertor (Sn, Z=50), the effect of impurity on the plasma performance is different. Since the threshold temperature for Sn sputtering is relatively low (5-6 eV), the conditions in divertor are such that plasma temperature stays close to threshold temperature leading to semi-detached conditions in the divertor. In spite of high radiation fraction for Sn target ($> 82\%$), seeding with additional impurities (Ne, Ar) is necessary to reduce the power to the targets to acceptable levels.

Acknowledgments

The authors would like to thank Dr T. P*ü*tterich from IPP Garching for providing them with atomic data for Sn.

This work has been carried out within the framework of the EUROfusion Consortium and has received funding from the Euratom research and training programme 2014-2018 under grant agreement No 633053. The views and opinions expressed herein do not necessarily reflect those of the European Commission. This scientific work was financed within the Polish framework of the scientific financial resources in 2015 allocated for realization of the international co-financed project.

References

[1] Loarte A., et al., Nucl. Fusion 47 (2007)
[2] Fusion Electricity - A roadmap to the realisation of fusion energy, F. Romanelli et al., EFDA, (2012)
[3] Eich T., et al., Phys. Rev. Lett.107 215001 (2011)
[4] Makowski M.A., et al Phys. Plasmas 19 , 056122 (2012)
[5] Shimomura et al. Nucl.Fus. 23 (1983) 869
[6] Kotschenreuther M., et al., Phys. Plasmas 14 72502 (2007)
[7] Kotschenreuther M., et al., 2004 *IAEA Fusion Energy Conference, Vilamoura, Portugal*IC/P6-43.
[8] Kotschenreuther M., et al., Phys. Plasmas 20 102507 (2007)
[9] Valanju P. M. et al., Phys. Plasmas 16 056110 (2009)
[10] Ryutov D. D., et al., Phys. Plasmas 14 064502 (2007)
[11] Apicella M.L, et al., J. Nucl. Mater. 363-365 1346 (2007)
[12] Apicella M.L, et al., Fusion Eng. Des. 75-79 351 (2005)
[13] Mazzitelli G., et al., Nucl. Fusion 51 073006 (2011)
[14] Mazzitelli G., et al., *34th EPS Conference on Plasma Phys. Warsaw, 2 - 6 July 2007* ECA Vol.31F, O-2.001 (2007)
[15] Mazzitelli G., et al., Fusion Engineering and Design 86 580 (2011)
[16] Mazzitelli G., et al., Journal of Nucl. Materials 463 1152 (2015)
[17] Jaworski M.A., et al. Nucl. Fusion 53 083032 (2013)
[18] Kotschenreuther M., et al., Nucl. Fusion 50 035003 (2010)
[19] Ryutov D. D., et al., Phys. Plasmas 15 092501 (2008)
[20] Ryutov D. D., et al., Plasma Phys. Control. Fusion 54 124050 (2012)
[21] Ryutov D. D., et al., Phys. Scr. 89 88002 (2014)
[22] Piras F., et al., Plasma Phys. Control. Fusion 51 055009 (2009)
[23] Piras F., et al., Phys. Rev. Lett.105 155003 (2010)
[24] H. Reimerdes, et al., PPCF 55 124027 (2013)

[25] W.A.J. Vijvers, et al., Nucl. Fusion, 54 023009 (2014)
[26] G.P. Canal, et al., Nucl. Fusion, 55 123023 (2015)
[27] Soukhanovskii V. A., et al., J. Nucl. Mater.415 S365 (2011)
[28] Soukhanovskii V. A., et al., Nucl. Fusion, 51 012001 (2011)
[29] Soukhanovskii V. A., et al., Phys. Plasmas 19 082504 (2012)
[30] Soukhanovskii V. A., et al., J. Nucl. Mater. 463 1191(2015)
[31] Soukhanovskii V. A., *3 Annual Meeting of the APS Division of Plasma PhysicsNew Orleans, LA, United States, LLNL report: October 23*, LLNL-CONF-663241 (2014)
[32] Calabro G.,et al. Nucl. Fusion 55 083005 (2015)
[33] Kemp R. , private communication
[34] R. Ambrosino, R. Albanese, Vertical Stability: WPPMI Final Report 2015, Annex A.
[35] R. Ambrosino, et al., "The DTT Device: Alternative Configurations", 29th Symposium on Fusion Technology (SOFT 2016), Prague, Czech Republic.
[36] Federici G.,et al. Fusion Eng. Des. 89 882 (2014)
[37] Knight P. J.,'A user guide to the PROCESS systems code', CCFE report (2013).
[38] ITER Physics Basis, Chapter 4: Power and particle control, Nucl. Fusion, 39, No. 12 (1999)
[39] Zagórski R,Gerhauser H., Phys. Scr.70 (Part 2/3) 173 (2004).
[40] Zagórski R., et al., J. Nucl. Mater 390-391 404 (2009).
[41] Zagórski R., et al., Nucl. Fusion 53 073030 (6pp) (2013)
[42] Wiesen S., EDGE2D/EIRENE code interface report, June, 2006, www.eirene.de
[43] Fichtmüller M., et al., Contributions to Plasma Physics, Volume 38, Issue 1-2, pages 284-289, (1998)
[44] Reiter D.,et al. , Fus. Sci Technol. 47 172 (2005)
[45] Rozhansky V.,et al. , Nucl.Fusion 49 025007 (2009)
[46] Bufferand H.,et al. , J. Nucl. Mater. 438 S445-S448 (2013)
[47] Lunt T.,et al. , Optimisation of the Snowflake Divertor by means of EMC3-Eirene simulations', to be submitted to Plasma Phys. Contr. Fusion
[48] Lisgo S.,et al. , J. Nucl. Mater. 337-339 139-145 (2005)
[49] Pericoli-Ridolfini V.,et al., Nucl. Fusion 53 (2013) 073030 (6pp) doi:10.1088/0029-5515/53/7/073030
[50] A.Scarabosio et al, J. Nucl. Mater 463 (2015) 49.
[51] B. Sieglin, et al., Plasma Phys. Control. Fusion 58 (2016) 055015.
[52] G.Rubino, et. al., *Comparative analysis of the SOL plasma in DEMO using EDGE2D/EIRENE and TECXY codes*, submitted to Nuclear Materials and Energy (2016).
[53] F.Subba, et. al., *Efficiency of non - standard divertor configurations in DEMO*, 22nd International Conference on Plasma Surface Interactions in Controlled Fusion Devices, 30 May - 3 June, 2016, Rome, Italy.
[54] B. Unterberg, FINAL-Report from FZJ for TA WP11-PEX-01-ACT3-01/FZJ/PS, Final reports ACT03 (Alternative target concepts) *https://idm.eurofusion. org/?uid=2LMHVE.*
[55] V.A. Evtikhin, Fusion Eng. Des. 49-50 (2000) 195-199.
[56] F.L. Tabares et al., 2nd ISLA Workshop 26-29 April 2011, 1B-3-Tabares-TJ-II.ppt, p.31 *http://nstx.pppl.gov/DragNDrop/Scientific_Conferences/ISLA%202011/ Session_I_Overview/.*
[57] Y. Nagayama, Fusion Eng. Des. 84 (7-11) (2009) 1380-1383.
[58] J.N. Brooks et al., Fusion Science and Technology, V. 47, (2005) 669-677
[59] J.N. Brooks et al., J. Nucl. Mater. 290-293 (2001) 185.
[60] T.D. Rognlien et al., J. Nucl. Mater. 290-293 (2001) 312.
[61] V. Pericoli-Ridolfini,et al., J. Nucl. Mater. **438** (2013) 414.
[62] V. Pericoli Ridolfini et al., Fusion Engineering and Design 88 (2013) 1677- 1681
[63] J.S. Hu et al., Fusion Engineering and Design, Volume 89, Issue 12, December 2014, Pages 28752885, doi:10.1016/j.fusengdes.2014.06.015
[64] R. Neu et al., Nucl. Fusion 45, 209 (2005).